

# Unambiguous path discrimination in a two-path interferometer

Yink Loong Len,<sup>1,2,\*</sup> Jibo Dai,<sup>1,2,†</sup> Berthold-Georg Englert,<sup>1,3,4,‡</sup> and Leonid A. Krivitsky<sup>2,§</sup>

<sup>1</sup>*Centre for Quantum Technologies, National University of Singapore, 3 Science Drive 2, Singapore 117543, Singapore*

<sup>2</sup>*Data Storage Institute, Agency for Science, Technology and Research,*

*2 Fusionopolis Way, #08-01 Innovis, Singapore 138634, Singapore*

<sup>3</sup>*Department of Physics, National University of Singapore, 2 Science Drive 3, Singapore 117542, Singapore*

<sup>4</sup>*MajuLab, CNRS-UNS-NUS-NTU International Joint Unit, UMI 3654, Singapore*

(Posted on the arXiv on 4 August 2017; this second version on 17 November 2017)

When a photon is detected after passing through an interferometer one might wonder which path it took, and a meaningful answer can only be given if one has the means of monitoring the photon's whereabouts. We report the realization of a single-photon experiment for a two-path interferometer with path marking. In this experiment, the path of a photon (“signal”) through a Mach–Zehnder interferometer becomes known by unambiguous discrimination between the two paths. We encode the signal path in the polarization state of a partner photon (“idler”) whose polarization is examined by a three-outcome measurement: one outcome each for the two signal paths plus an inconclusive outcome. Our results agree fully with the theoretical predictions from a common-sense analysis of what can be said about the past of a quantum particle: The signals for which we get the inconclusive result have full interference strength, as their paths through the interferometer *cannot be known*; and every photon that emerges from the dark output port of the balanced interferometer has a *known path*.

PACS numbers: 03.65.Ta, 42.50.Dv, 42.50.Xa

**Introduction** Vaidman’s three-path interferometer [1–3] is an asymmetric Mach–Zehnder interferometer (MZI) with a symmetric MZI inserted into one arm; weak interactions are used to mark the path of that particle through the interferometer. The emphasis is on photons detected at a particular one of the three exit ports, and Vaidman describes the pre- and post-selected ensemble by the two-state vector formalism that was introduced in Ref. [4]. To that he adds the interpretational rule that “the particle was in paths of the interferometer in which there is an overlap of the forward and backward evolving wave functions” [5], and then infers that each particle was inside the internal loop at intermediate times without, however, entering or leaving. In this narrative the particle was simultaneously at several places at the same time. While this account of the particle’s whereabouts is at odds with common sense, and also with more traditional ways of speaking about the past of a quantum particle, it is claimed that the experimental data reported in Refs. [2] and [3] support Vaidman’s narrative. This triggered a lively debate about these matters; see, for example, Refs.[4–33] in [6].

As we argued recently, the experimental data do not provide evidence in support of Vaidman’s interpretational rule [6]. Our conclusion follows from a careful examination of the path-information that can be extracted from the weak traces left by the particle when passing through the interferometer. When one acquires path knowledge by a fitting path-discriminating measurement, all particles in the pre- and post-selected ensemble have a known path through the interferometer — *one* known path for each particle — in full accordance with what common sense tells us.

An important ingredient in our analysis is a remarkable property of the inner balanced internal MZI: All particles that emerge from the dark output port — where they can only be found because the weak path marking slightly disturbs the balance of the MZI — have a knowable path through the MZI, despite the destructive interference that completely prevents particles from exiting at this output port if the balance is not upset. In the larger context of the three-path interferometer, then, these particles eventually recombine incoherently — an immediate consequence of their known path — with particles from the outer path at the final 2:1 beam splitter, and each particle detected after the beam splitter has a known path.

This prediction can be tested with fittingly prepared entangled photon pairs (“idler” and “signal”) [6]. The signal is fed into the MZI and detected at one of its exits, while the unambiguous discrimination of two polarization states of the idler provides information about the path taken by the signal. We report here a realization of such an experiment. It confirms the theoretical predictions, in particular that each signal detected at the dark output port has a known path through the MZI.

Experiments, in which the path of a quantum particle through an interferometer is marked by different states of internal degrees of freedom, have a long history. Important examples are neutrons and their spin [7]; atoms and their fine structure [8]; or photons and their polarization [9]. In other experiments, more closely related to our work, the paths of an interfering quantum particle are correlated with the degrees of freedom of auxiliary quantum systems: photon paths with atom states [10], electron paths with quantum-dot states [11], or photon

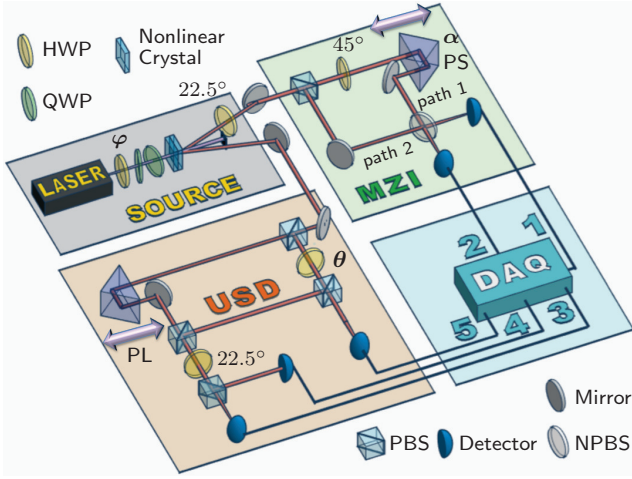


FIG. 1. Scheme of the experiment. The source emits wavelength-selected polarization-entangled photon pairs (signal and idler) in the state with the wave function of Eq. (2). On the signal side, a polarizing beam splitter (PBS) and a half-wave plate (HWP) convert the polarization qubit into the path qubit of a vertically polarized photon in a Mach-Zehnder interferometer (MZI). A phase shifter (PS) — the usual combination of a feedback-controlled piezo transducer and a translation stage — defines the phase  $\alpha$  of the MZI. When the nonpolarizing 50/50 beam splitter (NPBS) is removed, the signal's detection reveals its path. On the idler side, the setup of Clarke *et al.* [13] implements the unambiguous state discrimination (USD) of the two polarization states of the idler that are correlated with the signal paths [18]. The difference in optical length of the two paths of the loop is stabilized by a phase locker (PL), the analog of the PS on the signal side. The photons are fed to the detectors through single-mode fibers, and coincidences of any two detectors within the lapse of 5 ns are recorded by a data acquisition system (DAQ). The angle  $\theta$  the HWP at the USD is set such that detection of the idler by detectors D3 or D4 identifies unambiguously the path followed by the signal; see Table I for the coincidence probabilities of joint detection by the idler and signal detectors.

paths with partner-photon polarization states [12].

The unambiguous state discrimination (USD) of two nonorthogonal states was first demonstrated for photon polarization [13]. USD has also been realized for two states of a nuclear spin [14], three states of a path qutrit [15], four coherent states of a light mode [16], and up to 14 orbital-angular-momentum states of a photon [17].

**Scheme of the experiment** Figure 1 shows the scheme of the experiment. Our photon-pair source, described in details in Ref. [19], is of the kind pioneered by Kwiat *et al.* [20]. Spontaneous parametric down conversion creates photon pairs at 809.2 nm from a pump laser at 404.6 nm with the polarization wave function

$$\sin(2\varphi) \begin{bmatrix} 1 \\ 0 \end{bmatrix} \otimes \begin{bmatrix} 1 \\ 0 \end{bmatrix} + \cos(2\varphi) \begin{bmatrix} 0 \\ 1 \end{bmatrix} \otimes \begin{bmatrix} 0 \\ 1 \end{bmatrix} \quad (1)$$

in V/H basis, where the first factors in the tensor prod-

TABLE I. Coincidence probabilities of detecting the signal by detector D1 or D2 and the idler by detector D3, D4, or D5. In particle mode, the NPBS is removed from the MZI in Fig. 1 and the PS is of no consequence. In wave mode, the NPBS is in place and the probabilities of detecting the signal are  $2\pi$ -periodic in the interferometer phase  $\alpha$ .

MZI	signal detector	idler detector		
		D3	D4	D5
particle mode	D1	$\cos(2\varphi)^2$	0	$-\frac{1}{2} \cos(4\varphi)$
	D2	0	$\cos(2\varphi)^2$	$-\frac{1}{2} \cos(4\varphi)$
wave mode	D1	$\frac{1}{2} \cos(2\varphi)^2$	$\frac{1}{2} \cos(2\varphi)^2$	$-\cos(4\varphi) \cos(\frac{1}{2}\alpha)^2$
	D2	$\frac{1}{2} \cos(2\varphi)^2$	$\frac{1}{2} \cos(2\varphi)^2$	$-\cos(4\varphi) \sin(\frac{1}{2}\alpha)^2$

ucts are for the idler polarization and the second factors for the signal polarization. The angle parameter  $\varphi$  is adjusted by a half-wave plate (HWP) in the beam of the pump laser such that both photons are vertically polarized with probability  $\sin(2\varphi)^2$  or both are horizontally polarized with probability  $\cos(2\varphi)^2$ . Before leaving the source, the signal passes through a HWP set at  $22.5^\circ$ , which turns the wave function into

$$\begin{aligned} & \sin(2\varphi) \begin{bmatrix} 1 \\ 0 \end{bmatrix} \otimes \frac{1}{\sqrt{2}} \begin{bmatrix} 1 \\ 1 \end{bmatrix} + \cos(2\varphi) \begin{bmatrix} 0 \\ 1 \end{bmatrix} \otimes \frac{1}{\sqrt{2}} \begin{bmatrix} 1 \\ -1 \end{bmatrix} \\ &= \frac{1}{\sqrt{2}} \begin{bmatrix} \sin(2\varphi) \\ \cos(2\varphi) \end{bmatrix} \otimes \begin{bmatrix} 1 \\ 0 \end{bmatrix} + \frac{1}{\sqrt{2}} \begin{bmatrix} \sin(2\varphi) \\ -\cos(2\varphi) \end{bmatrix} \otimes \begin{bmatrix} 0 \\ 1 \end{bmatrix}. \end{aligned} \quad (2)$$

This is the polarization-entangled idler-signal state emitted by the source. The signal then enters the MZI, and the idler polarization is examined by USD.

On the signal side, the combination of the polarizing beam splitter (PBS) and the HWP at  $45^\circ$  converts the polarization qubit with the wave function  $\begin{bmatrix} v' \\ h' \end{bmatrix}$  into the path qubit of a vertically polarized photon with the wave function  $\begin{pmatrix} h' \\ v' \end{pmatrix}$  [21]. The phase shifter (PS) in path 1 imprints a phase  $\alpha$ , so that the probabilities of detecting the signal by detectors D1 or D2 behind the nonpolarizing 50/50 beam splitter (NPBS) are  $\frac{1}{2} |h'e^{i\alpha} + v'|^2$  and  $\frac{1}{2} |h'e^{i\alpha} - v'|^2$ , respectively. The MZI is balanced for  $v' = h'$  when  $\alpha = 0$ , with detector D2 probing the dark output port. See the Appendix for further details.

After the signal's polarization qubit is converted to a path qubit, we have the idler-signal wave function

$$\Psi = \frac{1}{\sqrt{2}} \begin{bmatrix} \sin(2\varphi) \\ -\cos(2\varphi) \end{bmatrix} \otimes \begin{pmatrix} 1 \\ 0 \end{pmatrix} + \frac{1}{\sqrt{2}} \begin{bmatrix} \sin(2\varphi) \\ \cos(2\varphi) \end{bmatrix} \otimes \begin{pmatrix} 0 \\ 1 \end{pmatrix}, \quad (3)$$

which exhibits the wave functions  $\begin{bmatrix} v \\ h \end{bmatrix} = \begin{bmatrix} \sin(2\varphi) \\ \mp \cos(2\varphi) \end{bmatrix}$

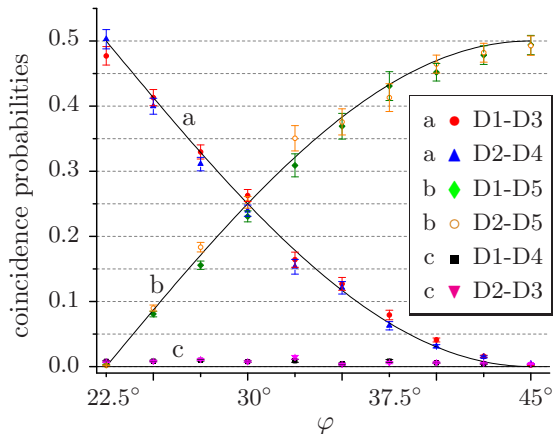


FIG. 2. USD outcomes and signal paths. The MZI is operated in particle mode (NPBS removed), so that a signal detected by D1 has taken path 2, and likewise for D2 and path 1. The solid curves are the theoretical predictions of Table I (top part). The data confirm in particular that the paths are correctly identified by clicks of D3 and D4: There are no D1-D4 and D2-D3 coincidences (curve “c”). The inconclusive outcomes are also as predicted: The D1-D5 and the D2-D5 coincidences are equally frequent (curve “b”). Here, and also in Figs. 3–4, the error bars indicate one standard deviation as obtained from suitable simulations of Poisson processes.

for the polarization states of the idler corresponding to signal path  $\begin{Bmatrix} 1 \\ 2 \end{Bmatrix}$  in the interferometer. These two idler states are told apart by the USD, the three-outcome measurement that projects on  $\phi_3$ ,  $\phi_4$ , or  $\phi_5$  with

$$\left. \begin{array}{l} \phi_3 \\ \phi_4 \end{array} \right\} = \frac{1}{\sqrt{2}} \begin{bmatrix} \cos(2\theta) \\ \mp 1 \end{bmatrix}, \quad \phi_5 = \begin{bmatrix} \sin(2\theta) \\ 0 \end{bmatrix}. \quad (4)$$

We set the HWP at the USD at angle  $\theta$  given by  $\cos(2\theta) = -\cot(2\varphi)$ , for  $22.5^\circ < \varphi < 45^\circ$ , and then have the coincidence probabilities listed in Table I for the detection of the signal in particle mode, i.e., with the NPBS removed from the MZI. Indeed, upon detecting the idler by D4, we know that the signal surely took path 1; likewise for D3 and path 2. We cannot infer the signal path, not at all, when the idler is detected by D5, which is the inconclusive outcome of the USD. Weak path marking is realized by  $\sin(2\varphi) \lesssim 1$  and  $0 \lesssim \cos(2\varphi) \ll 1$ , i.e.,  $\varphi \lesssim 45^\circ$ ; then, the probability for the inconclusive outcome, equal to  $1 - 2\cos(2\varphi)^2 = -\cos(4\varphi)$ , is close to 1.

**Testing the source and the USD** We test the quality of the two-photon source and the reliability of the USD by operating the MZI in particle mode (NPBS removed) so that detection of the signal by D1 or D2 identifies path 2 or path 1, respectively. Figure 2 shows the measured coincidence probabilities together with the theoretical values for an ideal experiment in Table I. The agreement between the theory and the experiment is very satisfactory. In particular, the virtual absence of D1-D4

and D2-D3 coincidences (curve “c”) confirms that the signal follows path 1 if D4 detects the idler, and likewise for path 2 and D3. Further, as predicted, we cannot infer the signal path if the idler is detected by D5 since the D1-D5 coincidences are as frequent as the D2-D5 coincidences (curve “b”). The data from another calibration experiment are reported in the Appendix.

**Sorted subensembles** The three outcomes of the USD identify three subensembles of signals and a corresponding way of blending the mixed signal state with the density matrix

$$\rho = \text{tr}_{\text{idler}}\{\Psi\Psi^\dagger\} = \frac{1}{2} \begin{pmatrix} 1 & -\cos(4\varphi) \\ -\cos(4\varphi) & 1 \end{pmatrix} \quad (5)$$

from three ingredients,

$$\begin{aligned} \rho &= \cos(2\varphi)^2 \begin{pmatrix} 1 & 0 \\ 0 & 0 \end{pmatrix} + \cos(2\varphi)^2 \begin{pmatrix} 0 & 0 \\ 0 & 1 \end{pmatrix} \\ &+ [-\cos(4\varphi)] \frac{1}{2} \begin{pmatrix} 1 & 1 \\ 1 & 1 \end{pmatrix}, \end{aligned} \quad (6)$$

associated with detecting the idler by D4, D3, or D5. The signals in the first subensemble follow path 1, those in the second subensemble follow path 2, whereas the path of a signal in the third subensemble is unknown — in fact, it is unknowable.

The combined effects of the PS in path 2 and the NPBS on the signal state yield the transformation

$$\rho \rightarrow \frac{1}{2} \begin{pmatrix} 1 - \cos(4\varphi)\cos(\alpha) & i\cos(4\varphi)\sin(\alpha) \\ -i\cos(4\varphi)\sin(\alpha) & 1 + \cos(4\varphi)\cos(\alpha) \end{pmatrix}, \quad (7)$$

so that

$$\begin{aligned} \left. \begin{array}{l} \text{prob(D1)} \\ \text{prob(D2)} \end{array} \right\} &= \frac{1}{2} [1 \mp \cos(4\varphi)\cos(\alpha)] \\ &= \frac{1}{2} \cos(2\varphi)^2 + \frac{1}{2} \cos(2\varphi)^2 \\ &+ [-\cos(4\varphi)] \begin{cases} \cos(\frac{1}{2}\alpha)^2 \\ \sin(\frac{1}{2}\alpha)^2 \end{cases} \end{aligned} \quad (8)$$

are the resulting probabilities for detecting the signal by D1 or D2. These probabilities exhibit interference fringes with visibility  $\mathcal{V} = |\cos(4\varphi)|$ , which equals the probability of obtaining the inconclusive result from the USD. For  $\varphi = 45^\circ$  (no path marking) and  $\alpha = 0$  (balanced MZI), there is perfect constructive interference at the D1 exit and perfect destructive interference at the D2 exit.

**Inconclusive USD outcome and fringe visibility** That the fringe visibility for the signals is equal to the probability of obtaining the inconclusive USD outcome for the idlers is not coincidental. We have a signal in the third subensemble of Eq. (6) if D5 detects the idler, and this subensemble consists of signals with utterly unknowable paths and full interference strength. The other two

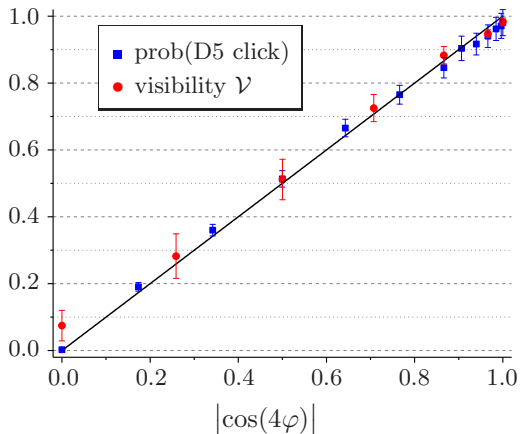


FIG. 3. Probability of obtaining the inconclusive USD outcome and MZI fringe visibility. The experimental data confirm that both quantities are equal to  $|\cos(4\varphi)|$ .

subensembles are made up of signals with a surely known path, and such signals do not contribute to the interference. The wave-mode coincidence probabilities in Table I and the corresponding ensemble sum in Eq. (8) summarize this matter. The statistical weight  $[-\cos(4\varphi)]$  of the third subensemble must, therefore, be equal to the fringe visibility.

These matters are confirmed by the data in Fig. 3. Indeed, we have evidence that (i) the probability of getting the inconclusive USD outcome for the idler (detection by D5) is equal to the fringe visibility for the signals (MZI in wave mode), and that (ii) both are equal to  $|\cos(4\varphi)|$  in terms of the source parameter  $\varphi$ .

In passing, we note that the probability of guessing the signal path right on the basis of the USD outcomes is

$$2 \cos(2\varphi)^2 + \frac{1}{2}[-\cos(4\varphi)] = \frac{1}{2}(1 + \mathcal{K}) \quad (9)$$

with  $\mathcal{K} = 2 \cos(2\varphi)^2 = |\cot(2\varphi)| \mathcal{D}$ . In the USD range of  $22.5^\circ < \varphi \leq 45^\circ$ , the path knowledge  $\mathcal{K} = 1 - \mathcal{V}$  thus gained is always less than the path distinguishability  $\mathcal{D} = \sqrt{1 - \mathcal{V}^2}$ . They are equal only for  $\varphi = 22.5^\circ$ , when  $\mathcal{V} = 0$  and  $\mathcal{K} = \mathcal{D} = 1$ . The purpose of the USD is different, however: It provides unambiguous knowledge about the signal path as often as possible, at the price of having no path knowledge at all whenever we obtain the inconclusive outcome.

**Balanced MZI with path marking** Finally, we address the situation encountered in Vaidman’s three-path interferometer [1–3] where the internal MZI is balanced and photons emerge from the dark output port only because the path marking disturbs the balance. So, we set the PS at  $\alpha = 0$  and look for signals detected by D2. The data in Fig. 4 confirm that the paths taken by these signals are known: There are D2-D3 and D2-D4 coincidences (path 2 and path 1, respectively; curve “a”)

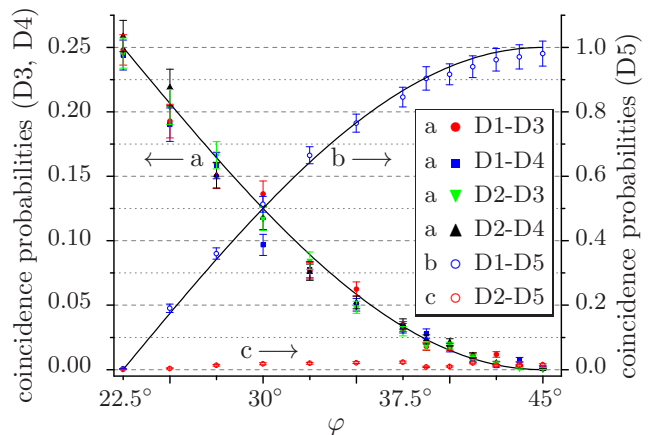


FIG. 4. Coincidence probabilities for the balanced MZI. The MZI is operated in wave mode (NPBS in place) and balanced (PS set at  $\alpha = 0$ ). The coincidence probabilities for the detector pairs D1-D3, D1-D4, D2-D3, and D2-D4 (curve “a”) are equal and agree well with the theoretical prediction in the bottom part of Table I (solid line). The  $\varphi$  dependence of the D1-D5 coincidence probability is also as expected (curve “b”) and, as predicted, there are no D2-D5 coincidences (curve “c”).

but no D2-D5 coincidences (curve “c”). Whenever there is an inconclusive outcome for the idler (detected by D5), the signal is detected by D1 — at the bright output port (curve “b”). By contrast, the signals with a known path (idler detected by D3 or D4) have an equal chance of being transmitted or reflected by the NPBS. This is demonstrated by the equal coincidence probabilities recorded for D1-D3, D1-D4, D2-D3, and D2-D4 (curve “a”). All of these observations are exactly as expected.

**Summary** Our experiment realizes a two-path interferometer with unambiguous path discrimination. All data are in very good agreement with the theoretical predictions in Ref. [6], which derive from the standard quantum formalism. We confirm, in particular, that each photon that emerges from the dark output port of the balanced interferometer has a known path. This confirmation has an immediate bearing on the experiments by Danan *et al.* [2] and Zhou *et al.* [3], inasmuch as it implies that all photons will have a known path through Vaidman’s three-path interferometer [1] if a suitable unambiguous path discrimination is performed.

**Acknowledgments** We are grateful for the insightful discussions with Hui Khoon Ng and the invaluable advice by Gleb Maslennikov. This work is funded by the Singapore Ministry of Education (partly through the Academic Research Fund Tier 3 MOE2012-T3-1-009) and the National Research Foundation of Singapore.

## APPENDIX

**Some details of the experiment** Figure 5 shows a schematic of the experiment depicted in Fig. 1, with

a detailed step-by-step account of how the polarization states of the signal and idler are changed as they traverse the setup until being finally detected by one of the five detectors.

On the idler side, the polarization qubit with the wave function  $\begin{bmatrix} v \\ h \end{bmatrix}$  is processed by the USD setup. Eventually, the idler is detected by D3 or D4 or D5 with the indicated probabilities.

On the signal side, the polarization qubit with the wave function  $\begin{bmatrix} v' \\ h' \end{bmatrix}$  is converted into the path qubit with the

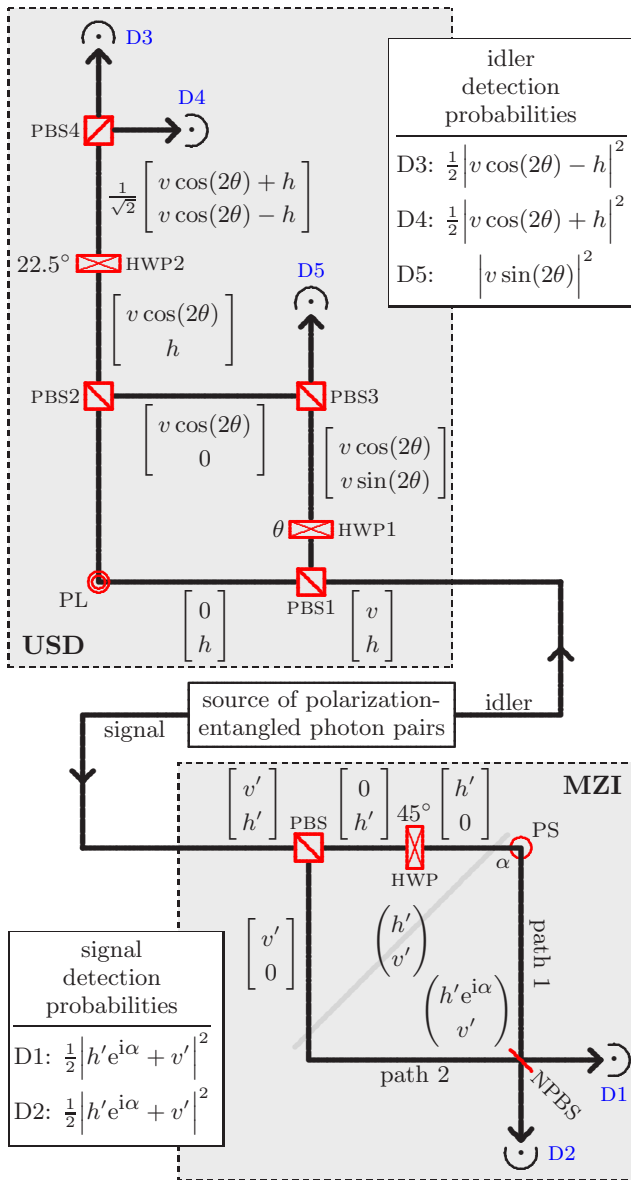


FIG. 5. A more detailed schematic of the experiment in Fig. 1. The polarization states of the signal and idler are indicated at the intermediate stages. The insets show the detection probabilities for the various detectors.

wave function  $\begin{pmatrix} h' \\ v' \end{pmatrix}$ , and the signal is eventually detected by D1 or D2. The indicated probabilities apply when the MZI is operated in wave mode (with the NPBS in place); in particle mode (NPBS removed), the detection probabilities are  $|v'|^2$  for D1 and  $|h'|^2$  for D2.

**Source of entangled photon pairs** The setup for the source of the polarization-entangled photon pairs is reported in our earlier work [19]. Two beta-borium borate (BBO) crystals of 2 mm thickness with orthogonal optic axes are cut at  $28.8^\circ$  for non-collinear frequency-degenerate phase matching. The BBOs are pumped by a frequency-stabilized continuous wave diode laser at a wavelength of 404.6 nm (Ondax, LM series). With non-collinear SPDC, the down-converted photons travel in different directions with a cone opening angle of  $4^\circ$ . Down-converted photons of narrow spatial bandwidth are collected into single-mode optical fibers using aspherical lenses with a focal length of 11 mm, placed at a distance of 900 mm from the BBOs. Using a half-wave plate (HWP) set at an angle  $\varphi$  and a pair of quarter-wave plates (QWPs) in the pump beam, we convert the pump polarization from  $\begin{bmatrix} 1 \\ 0 \end{bmatrix}$  to  $\cos(2\varphi) \begin{bmatrix} 0 \\ 1 \end{bmatrix} + \sin(2\varphi) \begin{bmatrix} 1 \\ 0 \end{bmatrix}$ , where  $\begin{bmatrix} 1 \\ 0 \end{bmatrix}$  and  $\begin{bmatrix} 0 \\ 1 \end{bmatrix}$  represent vertical and horizontal polarizations respectively. The first crystal produces pairs of vertically polarized photons from the pump's horizontal polarization component, while the second crystal produces pairs of horizontally polarized photons from the pump's vertical polarization component, giving us the signal-idler polarization wave function in Eq.(1) in the main text. After leaving the source, and before entering the MZI and USD respectively, polarization rotations in the optical fibers are compensated for by manual polarization controllers.

**Photon detection** After exiting the MZI and USD, at the various detection ports, the wavelengths of the signal and the idler are selected by interference filters with a central wavelength at 810 nm and a full width at half maximum of 10 nm. The photons are coupled into multi-mode fibers which are fed into single-photon detectors (Silicon Avalanche Photodiodes, quantum efficiency of about 50%, Qtools Twin QuTD). The data acquisition system (DAQ) is comprised of a time-to-digital converter (quTAU, Qtools), which we use to record coincidences of any two detectors within a coincidence time window of 5 ns.

**Phase locker and phase shifter** To implement the phase locker (PL) for the stabilization of the USD, we use an auxiliary HeNe laser at wavelength 632.8 nm. The locking laser is injected from the unused port of PBS2 in Fig. 5. As the optical elements have design wavelength at 810 nm but not 632.8 nm, there are non-zero amplitudes

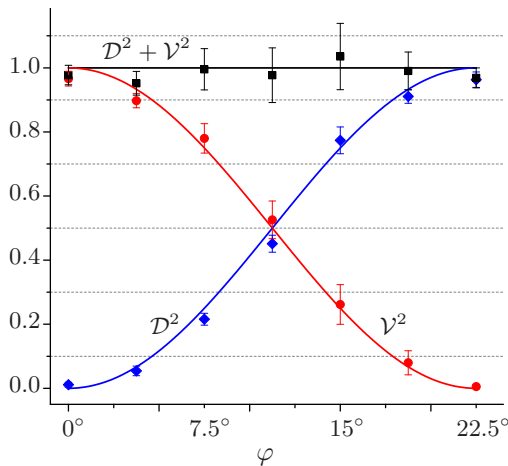


FIG. 6. Path distinguishability and fringe visibility. The plot shows the measured values of the squared path distinguishability,  $\mathcal{D}^2$ , and the squared fringe visibility,  $\mathcal{V}^2$ , as well as their sum. The solid lines are the theoretical predictions for an ideal experiment:  $\mathcal{D}^2 = \sin(4\varphi)^2$ ,  $\mathcal{V}^2 = \cos(4\varphi)^2$ ,  $\mathcal{D}^2 + \mathcal{V}^2 = 1$ .

of the HeNe laser propagating through the two arms of the interferometer in the USD. The two beams then interfere at PBS1. At the unused port of the PBS1, we install a HWP followed by a PBS, and measure the intensity at one of the output ports with a photodetector. The intensity is then converted to a voltage signal, and is fed to a home-built PID controller. The PID controller compares the signal with a fixed reference voltage which corresponds to the desired phase of the interferometer. If the signal deviates from the reference voltage, a feedback voltage is sent to the piezo transducer (Thorlabs model TLK-PZT1) attached to the phase locker mirror. The piezo transducer drives the mirror and brings the signal back to the reference voltage, and hence completes the locking and control of the phase of the interferometer.

The implementation of the phase shifter (PS) for the MZI is similar to the one for USD. We inject the HeNe laser from an acute angle reflecting off the interference filter in front of D1, which then enters the MZI. This allows us to lock and control the phase of the MZI using the interference signal of the HeNe laser at the unused port of the PBS.

**Testing the source and the MZI** Measurements of the fringe visibility  $\mathcal{V}$  and of the path distinguishability  $\mathcal{D}$  for various values of the source parameter  $\varphi$  serve as a test of the MZI, and also as another test of the photon-pair source. The data are reported in Fig. 6. Again, the comparison with the theoretical values is very satisfactory. This is further assurance that our experimental setup has no essential imperfections.

Here, the path distinguishability refers to the sorting of the signals by the outcome of the measurement for error minimization (MEM) on the idlers [22]. The MEM is an

orthogonal measurement that projects on the idler states  $\phi_{\pm} = \frac{1}{\sqrt{2}} \begin{bmatrix} 1 \\ \pm 1 \end{bmatrix}$ ; it is realized by the setup of Fig. 12 in [6] in the place of the USD in Fig. 1. The mixed state of the signals is now blended from two ingredients,

$$\rho = \frac{1}{2}\rho_+ + \frac{1}{2}\rho_-$$

$$\text{with } \rho_{\pm} = \frac{1}{2} \begin{pmatrix} 1 \mp \sin(4\varphi) & -\cos(4\varphi) \\ -\cos(4\varphi) & 1 \pm \sin(4\varphi) \end{pmatrix}. \quad (10)$$

Each subensemble has a probability of  $\frac{1}{2}(1 + |\sin(4\varphi)|)$  for the more likely signal path and  $\frac{1}{2}(1 - |\sin(4\varphi)|)$  for the less likely path. We always bet on the more likely path [23], and so guess the path right with a probability of

$$\frac{1}{2}(1 + |\sin(4\varphi)|) = \frac{1}{2}(1 + \mathcal{D}). \quad (11)$$

This identifies the path distinguishability  $\mathcal{D} = |\sin(4\varphi)|$ . Since we have  $\mathcal{V} = |\cos(4\varphi)|$  for the fringe visibility, it follows that the duality relation  $\mathcal{D}^2 + \mathcal{V}^2 \leq 1$  [23, 24] is saturated here.

There are, of course, many more ways of sorting the signals into subensembles. In particular, there is the quantum erasure sorting in which the subensembles consist of signals with unknowable paths and exhibit fully visible interference fringes; see Ref. [25] and references therein.

\* yinkloong@quantumlah.org

† dai.jibo@dsi.a-star.edu.sg

‡ cqtebg@nus.edu.sg

§ Leonid-K@dsi.a-star.edu.sg

- [1] L. Vaidman, Phys. Rev. A **87**, 052104 (2013).
- [2] A. Danan, D. Farfurnik, S. Bar-Ad, and L. Vaidman, Phys. Rev. Lett. **111**, 240402 (2013).
- [3] Z.-Q. Zhou, X. Liu, Y. Kedem, J.-M. Cui, Z.-F. Li, Y.-L. Hua, C.-F. Li, and G.-C. Guo, Phys. Rev. A **95**, 042121 (2017).
- [4] Y. Aharonov and L. Vaidman, Phys. Rev. A **41**, 11 (1990).
- [5] L. Vaidman, e-print arXiv:1610.04781 [quant-ph] (2016).
- [6] B.-G. Englert, K. Horia, J. Dai, Y. L. Len, and H. K. Ng, Phys. Rev. A **96**, 022126 (2017).
- [7] J. Summhammer, G. Badurek, H. Rauch, and U. Kischko, Phys. Lett. **90A**, 110 (1982).
- [8] S. Dürr, T. Nonn, and G. Rempe, Nature (London) **395**, 33 (1998).
- [9] P. D. D. Schwindt, P. G. Kwiat, and B.-G. Englert, Phys. Rev. A **60**, 4285 (1999).
- [10] U. Eichmann, J. C. Bergquist, J. J. Bollinger, J. M. Gilligan, W. M. Itano, D. J. Wineland, and M. G. Raizen, Phys. Rev. Lett. **70**, 2359 (1993).
- [11] E. Buks, R. Schuster, M. Heiblum, D. Mahalu, and V. Umansky, Nature (London) **391**, 871 (1998).
- [12] T. J. Herzog, P. G. Kwiat, H. Weinfurter, and A. Zeilinger, Phys. Rev. Lett. **75**, 3034 (1995).

- [13] R. B. M. Clarke, A. Chefles, S. M. Barnett, and E. Riis, *Phys. Rev. A* **63**, 040305 (2001).
- [14] G. Waldherr, A. C. Dada, P. Neumann, F. Jelezko, E. Andersson, and J. Wrachtrup, *Phys. Rev. Lett.* **109**, 180501 (2012).
- [15] M. Mohseni, A. M. Steinberg, and J. A. Bergou, *Phys. Rev. Lett.* **93**, 200403 (2004).
- [16] F. E. Becerra, J. Fan, and A. Migdall, *Nat. Commun.* **4**, 2028 (2013).
- [17] M. Agnew, E. Bolduc, K. J. Resch, S. Franke-Arnold, and J. Leach, *Phys. Rev. Lett.* **113**, 020501 (2014).
- [18] We found it easier to stabilize the loop in the USD setup of Clarke *et al.* than in the setup of Fig. 11 in [6].
- [19] J. Dai, Y. L. Len, Y. S. Teo, L. A. Krivitsky, and B.-G. Englert, *New J. Phys.* **15**, 063011 (2013).
- [20] P. G. Kwiat, E. Waks, A. G. White, I. Appelbaum, and P. H. Eberhard, *Phys. Rev. A* **60**, R773 (1999).
- [21] As we did in [6], we use columns with round brackets for path-qubit wave functions and columns with square brackets for polarization-qubit wave functions.
- [22] C. W. Helstrom, *Quantum Detection and Estimation Theory* (Academic Press, New York, 1976).
- [23] B.-G. Englert, *Phys. Rev. Lett.* **77**, 2154 (1996).
- [24] G. Jaeger, A. Shimony, and L. Vaidman, *Phys. Rev. A* **51**, 54 (1995).
- [25] B.-G. Englert and J. A. Bergou, *Opt. Commun.* **179**, 337 (2000).